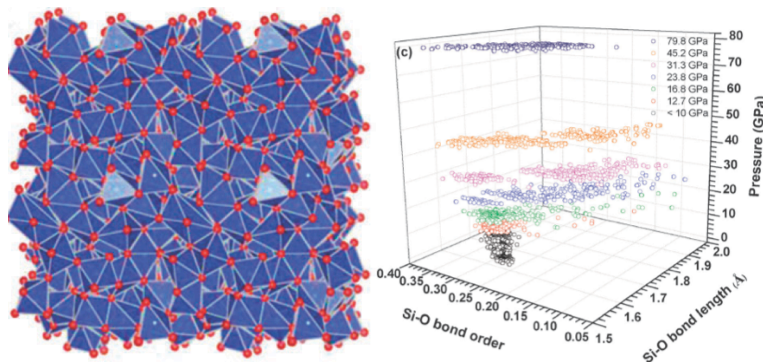


Analyzing the phase transition of amorphous-to-amorphous SiO₂ under various conditions



“Silicon dioxide is one of the most important noncrystalline and abundant materials of the Earth; Silicon dioxide glass can be viewed as a model system to further our understanding of the general features and properties amongst inorganic glasses with no long range order,” says Dr. Neng Li, the lead author of the article **Densification of a continuous random network model of amorphous SiO₂ glass**. In the past year Dr. Li *et al.* from the University of Missouri-Kansas City performed theoretical calculations of SiO₂ glass under pressures ranging from 0 to approximately 80 GPa. Like liquid-solid transitions, or structural changes in crystalline solids that occur with increased pressure, previous experimental and theoretical work found that an amorphous to amorphous transition occurs with an increased pressure. There is some confusion from the experimental and theoretical work done in regards to the range of pressures that this phase transition occurs, and Dr. Li noted that it is indeed puzzling that there are different experimental ranges found for the phase transition of an identical material. Previous theoretical work done showed that the 4-fold to 6-fold coordination transition occurs between 10 and 22 GPa, but other results contradicted this result and predicted that the transition should have started at 30 GPa. The pressure range chosen by Dr. Li *et al.* was appropriate to determine the correct pressure for the

phase transition. “The contradictions in previous studies may be due to the limited number of atoms in the models used,” says Dr. Li.

There has been an increased interest to study amorphous silica under high pressure in recent literature not only in condensed matter physics, but in material science and geophysics. The contradictions in previous work behind the range of pressures also supplies additional motivation to properly understand the phase transitions and structure of amorphous silica.

To begin their calculations, Dr. Li *et al.* built a near-perfect low density continuous random network (CRN) for SiO₂ glass at 0 GPa. Since their model contained 1296 atoms, fully relaxing the system without breaking any bonds or producing over-coordinated atoms is not a trivial task. Once the system was fully relaxed, the density found agreed well with experiment; both yielding densities found to be 2.20 g/cc. The molecular dynamic simulations and calculations were performed using density functional theory (DFT) based *ab initio* methods; the two packages used include the Vienna *ab initio* simulation package (VASP) and orthogonalized linear combination of atomic orbitals methods (OLCAO). In order to understand the atomistic phase transitions, a full analysis of real-space pair distribution functions (RPDF) were performed as the pressure was increased in the system. The RPDF’s tell you the proba-

bility of where you'll find another atom next to a selected atom (i.e. Si-O, O-O, or Si-Si). Dr. Li *et al.* found that up to a pressure range of 20-25 GPa, the RPDF's maintained the same features as at zero pressure indicating no major changes in the structure. In the pressure range of 25-35 GPa, the first peak position of the Si-Si pair shifts noticeably to larger distance, signalling a possible coordination change for Si. The O-Si-O bond angle was also studied and in the pressure range exceeding 25 GPa, angles that were found suggested that polyhedral units found were more likely to be a mixture of tetrahedrons and octahedrons rather than all tetrahedral. An analysis of the Si-O bond length was also done, and the theoretical values found agreed well with other experimental and theoretical data; as the pressure increased beyond 15 GPa, the Si-O bond length increased until reaching a maximum at 30 GPa. Anything beyond 30 GPa, the bond length begins to decrease gradually due to the compression of the newly formed Si-O octahedra. Lastly, and most importantly, Dr. Li *et al.* performed analysis on the coordination number (CN) versus pressure for Si-O; this tells you the number of Si-O molecules that are nearest neighbours to any other selected Si-O molecule. As expected the coordination number increased as the pressure was increased, and a maximum value of 5.8 was reached at the maximum pressure of 80 GPa. The change in the coordination number was found to be in the pressure range of 20-25 GPa, and a coordination number of 6 was never reached, even at 80 GPa. Dr. Li mentioned that the completion of the phase transformation can vary considerably depending on the nature of the initial glass structure, and the evolution with increasing pressures. Extended examination of the CN-pressure plot indicates there may be an even denser phase with a higher coordination number close to 148 GPa. In addition to properties relating to the phase transitions, theoretical calculations for the refractive index of the SiO₂ glass were performed as a function of pressure for the first time, and they agree well with experimental data. In the future Dr. Li hopes to continue work with SiO₂ performing modelling of nano-dimensional amorphous silicon dioxide, and to find the structural properties of point defects in amorphous SiO₂.

1) What is your academic background? What institution are you at currently and what are your research interests?

Response: I got Ph.D. in condensed physics in 2011. Now, I am assistant professor in Shenzhen Institutes of Advanced Technology, China. The main research interests are the electronic, mechanical, structural, optical, vibrational, and magnetic properties of ordered and disordered solids, with focus on materials with complex structures. As the primary vehicle for my research I use first-principles methods that are based on density functional theory, with support from other simulation tools (molecular dynamics such as LAMMPS). The orthogonalized linear combination of atomic orbitals (OLCAO) method is the main computational code used. Other ab initio packages and methods such as Vienna Ab initio simulation package (VASP) are also extensively used in conjunction with the OLCAO method. Our repertoire of projects include investigation of electronic structure and bonding (including H-bonding), characterization via spectroscopic calculations, determination of mechanical and elastic properties, tensile and compression experiments on supercomputers, research on lattice dynamics, phonon spectra, phases diagrams and thermodynamic properties, exploring the long-range interactions (electrostatic, polar, and van der Waals) in biomolecular systems, transport properties in complex ceramics, and materials under extreme conditions of high temperature and pressure. I am also actively developing robust, accurate, and efficient computational tools with unique predictive power.

2) What was the motivation behind your research of SiO₂?

Response: As one of the most important noncrystalline materials and abundant components of the Earth, silica garners intense research attraction in past decades. Silica (α -SiO₂) glass can be viewed as a model system to further our understanding on the general features and properties amongst inorganic glasses with no long range order. Recently, there has been increased interest in the silica glass structures subject to extreme high pressures (420 GPa) due to its importance not only in condensed matter physics but also in material science and geophysics, especially on the subject of amorphous to amorphous phases transition (AAPT). Experimentally, numerous advanced materials characterization tools and techniques have been employed to characterize the complex behaviour of pressurized silica glass such as X-ray diffraction, neutron diffraction, and Raman and Brillouin spectroscopy. Additionally, there has been a steady increase in the number of theoretical studies on the subject based on molecular dynamic (MD) simulations. In spite of these efforts, the full mechanism of densification process of silica glass at the atomistic level and its detailed impact on the local structure is still not fully understood. This is quite evident from the seemingly conflicting conclusions drawn from different types of experiments as well as

theoretical studies concerning the transition pressure associated with the 6-fold coordinated Si. It is indeed quite puzzling that there exists such a variety of different interpretations for the onset pressures for an apparently identical material.

3) What was the procedure followed for your research of SiO₂? What experimental/theoretical techniques did you use? What information did you want to learn from your system of molecules?

Response: First, we build a large a nearly perfect continuous random network (CRN) model of amorphous SiO₂ (a-SiO₂) glass with 1296 atoms and periodic boundary conditions. Then fully relaxed using VASP to high accuracy and the final model with density of 2.20 g/cm³ and very small bond length and bond angle distortions is obtained. Then, full electronic calculation using OLCAO with a large basis, and optical and mechanical properties calculations. The main shortcomings encountered in these studies appear to be the lack of precise quantification of the short range and intermediate range structures of the glass, primarily due to the limited number of atoms in the models used in these studies. Furthermore, since the simulated glass structure was typically procured from a rapidly cooled melt via molecular dynamics simulations, the obtained quenched glass structures inevitably contain a significant portion of defective structures such as broken bonds, over- or under-coordinated Si and O atoms, and large distortions in its bond length (BL) and bond angle (BA) distributions. Such defective features in the glass model often mask the key features in the structural characterization and the physical properties calculated based on such models. Thus it is essential to perform systematic density functional theory (DFT) study with a sufficiently large, but also a nearly perfect continuous random network (CRN) model of silica glass with small BL and BA distortions and no defects. Such rigorous calculations on a near-perfect CRN model can minimize the uncertainties induced by defects in the interpretation of the calculated results. The objective of the present work is therefore to provide a comprehensive assessment of many different aspects of the measurable properties on a-SiO₂ upon densification utilizing a nearly perfect CRN model of silica glass using the ab initio constant pressure simulation technique.

4) What were the main results that you obtained from your calculations? What results were you most interested in or satisfied with?

Response: By assessing a full spectrum of properties including atomic structure, bonding characteristics, effective charges, bond order values, electron density of states, localization of

wave functions, elastic and mechanical properties, and interband optical absorption at each pressure, we reveal the pertinent details on the structural, mechanical and optical characteristics of the glass model under pressure. They all confirm the central theme that amorphous to amorphous phase transformation (AAPT) from a low-density state to a high-density state is at a pressure between 20 and 35 GPa in this nearly ideal a-SiO₂ network. This pressure range represents an upper limit for such a transition in vitreous silica. The phase transformation roots from the change of Si–O bonding from a mixture of ionic and covalent nature at low pressure to a highly covalent bonding under high pressure. In addition, the calculated theoretical refractive index of the glass model as a function of the pressure is reported for the first time and in good agreement with the available experimental data.

5) What do you want other researchers to take away from your work when they read your research?

Response: One can apply classical MD technique to quench the present near-perfect CRN model from high temperature to investigate the effect of breaking the more ordered network structure with the creation of under or over coordinated atoms. It is also desirable to extend the simulation to decompressing process and in using smaller pressure increments to further improve accuracy.

6) Will you be doing any more work with SiO₂? What are your future plans for research in this area?

Response: It is fitting to comment on further research than can be anticipated using this nearly perfect random network model and the computational approach we used in studying the properties of materials under densification. The more details please refer to the second part of the “conclusion” section.

7) What do you hope to learn from researching amorphous SiO₂ in the future?

Response: In the future, I would like to perform modelling of nano dimensional amorphous silicon dioxide, and structural properties of point defects in amorphous SiO₂

Densification of a continuous random network model of amorphous SiO₂ glass

Neng Li, Ridwan Sakidja, Sitaram Aryal and Wai-Yim Ching*

Cite this: *Phys. Chem. Chem. Phys.*, 2014, **16**, 1500

Received 29th July 2013,
Accepted 28th October 2013

DOI: 10.1039/c3cp53192a

www.rsc.org/pccp

We have investigated the mechanism of densification of a nearly perfect continuous random network (CRN) model of amorphous SiO₂ (a-SiO₂) glass with 1296 atoms and periodic boundary conditions. The model has no under- or over-coordinated atoms and small bond length and bond angle distributions. This near-perfect model is systematically densified up to a pressure of 80 GPa using *ab initio* constant-pressure technique. By assessing a full spectrum of properties including atomic structure, bonding characteristics, effective charges, bond order values, electron density of states, localization of wave functions, elastic and mechanical properties, and interband optical absorption at each pressure, we reveal the pertinent details on the structural, mechanical and optical characteristics of the glass model under pressure. They all confirm the central theme that amorphous to amorphous phase transformation (AAPT) from a low-density state to a high-density state is at a pressure between 20 and 35 GPa in this nearly ideal a-SiO₂ network. This pressure range represents an upper limit for such a transition in vitreous silica. The phase transformation roots from the change of Si–O bonding from a mixture of ionic and covalent nature at low pressure to a highly covalent bonding under high pressure. In addition, the calculated theoretical refractive index of the glass model as a function of the pressure is reported for the first time and in good agreement with the available experimental data.

1. Introduction

As one of the most important noncrystalline materials and abundant components of the Earth, silica garners intense research attraction in past decades.^{1–3} Silica (a-SiO₂) glass can be viewed as a model system to further our understanding on the general features and properties amongst inorganic glasses with no long range order. Recently, there has been increased interest in the silica glass structures subject to extreme high pressures (>20 GPa) due to its importance not only in condense matter physics but also in material science and geophysics,^{4–6} especially on the subject of amorphous to amorphous phases transition (AAPT). Experimentally, numerous advanced materials characterization tools and techniques have been employed to characterize the complex behavior of pressurized silica glass such as X-ray diffraction,^{7–9} neutron diffraction,¹⁰ Raman and Brillouin spectroscopy.^{11–15} Additionally, there has been a steady increase in the number of theoretical studies on the subject based on molecular dynamic (MD) simulations.^{10,16–23} In spite of these efforts, the full mechanism of densification process of silica glass at the atomistic level and its detailed impact on the local structure is still not fully understood. This is quite evident from the seemingly conflicting conclusions

drawn from different types of experiments as well as theoretical studies concerning the transition pressure associated with the 6-fold coordinated Si. According to the comparative study on the O K-edge X-ray Raman scattering spectra between silica glass and crystalline quartz/stishovite, it was suggested that a change in the Si environment from 4-fold to 6-fold coordination occurs between 10 to 22 GPa.²⁴ But based on the acoustic velocity data obtained from Brillouin scattering, it was reported that the onset transition should have started instead at 30 GPa, and that the 6-fold coordination for Si can only be sustained up to a high pressure of 140 GPa.²⁵ In contrast, a study on the Si L-edge from X-ray Raman scattering data found no significant change in the spectral features and concluded that the 4-fold coordination environment of Si should remain up to 74 GPa.⁹ It is indeed quite puzzling that there exists such a variety of different interpretations for the onset pressures for an apparently identical material.

The main shortcomings encountered in these studies appear to be the lack of precise quantification of the short range and intermediate range structures of the glass, primarily due to the limited number of atoms in the models used in these studies. Furthermore, since the simulated glass structure was typically procured from a rapidly cooled melt *via* molecular dynamics simulations, the obtained quenched glass structures inevitably contain a significant portion of defective structures such as broken bonds, over- or under-coordinated Si and O atoms,

Department of Physics and Astronomy, University of Missouri-Kansas City, Kansas City, MO 64110, USA. E-mail: Chingw@umkc.edu

and large distortions in its bond length (BL) and bond angle (BA) distributions. Such defective features in the glass model often mask the key features in the structural characterization and the physical properties calculated based on such models. Thus it is essential to perform systematic density functional theory (DFT) study with a sufficiently large, but also a nearly perfect continuous random network (CRN) model of silica glass with small BL and BA distortions and no defects. Such rigorous calculations on a near-perfect CRN model can minimize the uncertainties induced by defects in the interpretation of the calculated results. The objective of the present work is therefore to provide a comprehensive assessment of many different aspects of the measurable properties on a-SiO₂ upon densification utilizing a nearly perfect CRN model of silica glass using the *ab initio* constant pressure simulation technique. The organization of this paper is as follows: in Section II, we provide a brief account on this fully relaxed near-perfect CRN model of a-SiO₂ and outline the method of calculation. The results and the detailed analysis of the physical properties of the model under pressure are presented and discussed in Section III. These include the information on the changes in the structure, the elastic and mechanical properties, the electronic structure and electron states, the effective charges and bonding characteristics, and the optical properties as a function of pressure. Finally, in the last section, a briefly summary and the prospect of further applications of this model are presented.

II. Structural model

The polyhedron view of our fully relaxed near-perfect CRN model for a-SiO₂ glass at low density amorphous (LDA) structures (0 GPa) and its high density amorphous (HDA) structures at 80 GPa are shown in Fig. 1a and b respectively. Our initial zero-pressure model is the one used in the past^{26,27} that was developed over a long period of time and can be traced back to the modeling of a-Si. This model has a long history being applied in the studies of electronic and vibrational properties of a-SiO₂ glass. The model is periodic and contains 432 SiO₂ molecules (1296 atoms) without the presence of broken bonds or over- and under-coordinated Si or O atoms. In the previous studies for the electron and phonon states of this model, it was relaxed by four sets of classical pair potentials of a simple Buckingham form with parameters derived from a variety of different approaches.

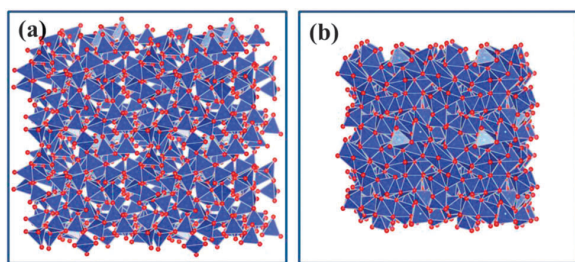


Fig. 1 The polyhedral structure of the near-perfect CRN model of a-SiO₂ glass at: (a) zero pressure; (b) densified structure at 79.8 GPa.

They are: (1) a pair potential derived by van Beest, Kramer and Santen based on quantum-chemical calculation of H₄SiO₄ cluster,²⁸ (2) potential derived by Tsuneyuki and co-workers using a Hartree-Fock type calculation on [SiO₄]⁻⁴,²⁹ (3) a three-body potential by Sanders, Leslie, and Catlow³⁰ within a shell-model description for three-body interaction; and (4) a potential developed by Kramer *et al* using a mixture of self-consistent field calculations and empirical procedures.³¹ In the present study, the previous model^{26,27} is fully relaxed with a high precision using DFT-based method with a periodical boundary constraint and no imposed symmetry restrictions. This resulted in a glass model with an even smaller BL and BA distortions than the previous model^{26,27} and with a near-perfect tetrahedral structure as shown in Fig. 1a. It should be pointed that the matching of the periodic boundary for a-SiO₂ with strong directional bonding to yield a near-perfect ideal CRN model is a nontrivial task. In fact, this has been one of the main difficulties encountered in a typical silica glass model generated from molecular dynamics simulations or other technique.²⁰ In spite of no restriction imposed on the shape and size on the model in the relaxation process (to be described below), the final mass density of the present model is found to be 2.202 g cm⁻³ in excellent agreement with experimental density of 2.20 g cm⁻³. Table 1 summarizes some of the basics structural characteristics of this model. Based on this zero pressure model for a-SiO₂ glass, we have obtained the interband optical spectrum and found it to be in quite good agreement with the experimental results.³²⁻³⁴ Previously, such attempt yielded undesirable result due to many approximations made because of the unavailability of sufficient computing power for such demanding calculations.²⁷

III. Computational details

To perform efficient electronic structure simulations on the densification process, we employed two well established DFT-based *ab initio* methods; the plane-wave projector-augmented wave method as implemented in Vienna *ab initio* simulation package (VASP)^{35,36} and the orthogonalized linear combination of atomic orbitals methods (OLCAO)^{37,38} as implemented in the OLCAO package using local density approximation (LDA) of the density functional theory.^{39,40} This method has been applied to many other complex materials.^{26,27,37,38,41-44} The structural relaxation, mechanical and elastic properties are carried out by using VASP whereas the electronic structure, bonding characteristics, localization analysis and optical properties are calculated using the local orbital-based OLCAO method. For structural relaxation, the PAW-PBE potential⁴⁵ with generalized gradient approximation (GGA) as supplied in the VASP is used for the exchange-correlation potential. We used a cutoff energy of 600 eV, a relatively high accuracy for the ground state electronic convergence criterion (10⁻⁵ eV) and force convergence limit (10⁻² eV Å⁻¹). The stress level of the final equilibrium structure is less than 0.1 GPa. The relaxation of the present model imposes no restrictions on the volume and lattice vectors of periodic supercell. Since our model is sufficiently large,

Table 1 Physical characteristics of the near-perfect CRN model for a-SiO₂ glass upon densification

	Pressure (GPa)											
	0.0	1.3	2.6	4.0	6.4	9.2	12.7	16.8	23.8	31.3	45.2	79.8
<i>a</i> (Å)	27.43	27.16	26.89	26.61	26.06	25.52	24.97	24.42	23.60	22.50	21.95	21.13
<i>b</i> (Å)	25.38	25.11	24.85	24.60	24.09	23.58	23.08	22.57	21.81	20.79	20.29	19.53
<i>c</i> (Å)	28.31	28.02	27.73	27.47	26.89	26.32	25.76	25.19	24.34	23.21	22.64	21.80
Density (g cm ⁻³)	2.19	2.26	2.33	2.40	2.56	2.73	2.91	3.11	3.45	3.98	4.30	4.81
<i>V/V</i> ₀	1.00	0.97	0.94	0.91	0.86	0.80	0.75	0.71	0.64	0.55	0.51	0.46
<i>ρ/ρ</i> ₀	1.00	1.03	1.06	1.10	1.17	1.24	1.33	1.42	1.57	1.82	1.96	2.19
Average BL (Å)	1.629	1.627	1.625	1.624	1.621	1.620	1.618	1.733	1.815	1.965	2.084	2.193
Average BA (deg.)												
O-Si-O (θ)	109.46	109.46	109.46	109.46	109.45	109.45	109.44	108.53	107.96	106.20	105.06	104.37
Si-O-Si (φ)	146.36	144.09	141.88	139.81	135.95	132.47	129.49	126.11	121.72	118.04	116.29	115.36

only one *K*-point at $\Gamma(0,0,0)$ is used. In the OLCAO method, the solid state wave functions are expanded in atomic orbitals which consist of Gaussians type orbitals (GTOs) and spherical harmonics appropriate for the angular momentum quantum number. Three types of basis set were used. The full basis (FB), which consists of the core orbitals, occupied valence orbitals, and the next empty shell of unoccupied orbitals for each atom, is used for the determination of the self-consistent potential and subsequent calculations of band structure and density of states (DOS). In the calculation of optical conductivities, an extended basis (EB) set was used, which include one additional shell of empty orbitals to improve the accuracy of the higher states in the conduction band. On the other hand, for the effective charge and bond order calculations using Mulliken analysis,⁴⁶ a minimal basis (MB) was used which provides a more localized basis for such analysis. The versatility of using different basis sizes for different purposes is instrumental in enabling the OLCAO method to have high efficiency and accuracy for calculations of a variety of properties. A full basis set consisting of atomic orbitals of Si (1s, 2s, 3s, 4s, 2p, 3p, 4p, 3d) and O (1s, 2s, 3s, 2p, 3p) is used for the self-consistent electronic structure calculation and an extended basis with additional shells of orbitals in Si and O atomic basis set is employed for optical properties calculation. The final secular equation with the extended basis set has a dimension of $23\,328 \times 23\,328$ after core orthogonalization procedure.^{37,38} All energy eigenvalues and eigenvectors are obtained at the Γ point and used for the properties calculations and analysis.

IV. Results and discussions

A. Structural properties of a-SiO₂ under pressure

As we mentioned it at the previous section, Fig. 1a and b show that the polyhedron structure of the near-perfect CRN model for a-SiO₂ glass under zero pressure and the compressed model at 80 GPa, the highest pressure in the present study, respectively. The zero-pressure model is characterized by the network linkage of SiO₄ tetrahedral units as expected whereas in the highly compressed model, this is no longer the case (further details on the glass structures will be elaborated in the next sub-section). It can be seen from Fig. 2 that the silica density

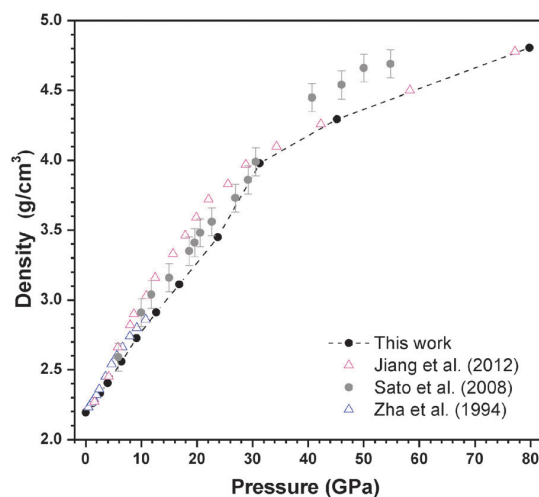


Fig. 2 Comparison of calculated densities as a function of pressure (black solid circle) with experimental measured by Zha *et al.* (ref. 47, blue open triangle) and Sato *et al.* (ref. 51, dark solid circle), and MD simulation by Jiang *et al.* (ref. 49, red open triangle).

increases with pressure in a good agreement with those reported in the previous works.^{47–49} Also to be noted in Fig. 2 is that in our work, compressions beyond 20 GPa yield a slightly less densities than those found in experiments of Zha⁴⁷ and Sato.⁴⁸ We attributed this to the fact that our glass model is more resistant to the applied compression possibly due to the absence of structural defects which are usually present in real glass samples.

In order to shed more light on the nature of the amorphous-to-amorphous phase transition in the a-SiO₂ glass at the atomistic level, we analyze the structural changes in terms of the real-space pair distribution functions (RPDF). The calculated total and partial RPDFs for Si-O, Si-Si, and O-O pairs are shown in Fig. 3. At zero pressure, the RPDF for Si-O pair has one well-resolved peak at 1.62 Å corresponding to the average Si-O separations in agreement with previous works.^{50,51} The RPDFs of Si-Si and O-O pairs are broader indicative of the amorphous structure that lacks the long-range order. Up to a pressure range of 20–25 GPa, the total (Fig. 3a) and Si-O partial (Fig. 3b) RPDFs maintain the same features as at zero pressure indicating the integrity of the network structure has not changed.

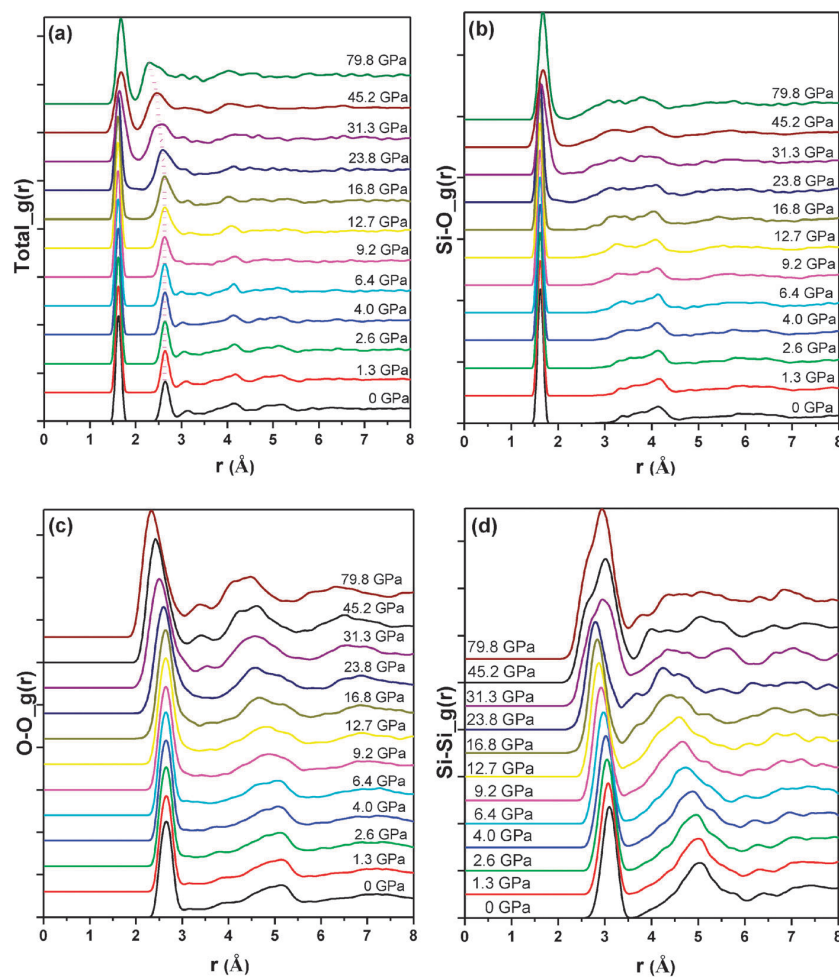


Fig. 3 Calculated total and partial real-space partial-pair distribution functions (RPDF) vs. pressure. (a) Total, (b) Si–O, (c) O–O, and (d) Si–Si.

On the other hand, Fig. 3c and d show the first peak positions for the O–O and Si–Si pairs shift to shorter distances showing the tightening in the packing of the network. When the pressure exceeds 25–35 GPa range, the intensity of the other peaks tends to be broader due to the widening of the Si–O pair distribution shown in Fig. 3b. The intensity of the second peak of the total RDF (Fig. 3a) on the other hand, exhibits a sharp decrease to a shorter distance. This large shift is mainly due to the significant change in the O–O pair distribution (see Fig. 3c). Moreover, within this range of pressure, the first peak position of the Si–Si pair (Fig. 3d) shifts noticeably to a larger distance, signaling a possible initiation of coordination change for Si. Beyond this pressure range, we note the overlapping of the first peak of the Si–Si peak with other peaks at a larger distance. The degree of overlapping increases with pressure. In fact, even up to the maximum pressure studied (80 GPa), such overlapped peaks do not merge into a single broad peak, demonstrating the retention of some of the original Si coordination environment.

The O–Si–O and Si–O–Si bond angle distributions (BAD) in the model as a function of pressure are shown in Fig. 4a and b.

The distribution for the Si–O–Si bridging angles is very broad and centered at around 148° at zero pressure accordant with the fact that the bridging angles are very flexible. On the other hand, the O–Si–O distribution has a single peak centered at the tetrahedral angle of 109.5° consistent with other previous studies. Upon compression with a pressure exceeding the range of 20–25 GPa, the average O–Si–O angle gradually decreases with a concomitant increase in the spread. The appearance of O–Si–O angles at less than 60° and larger than 150° in the distribution at high pressure implies the polyhedral units in the model are no longer tetrahedral and likely to be a mixture of tetrahedrons and octahedrons. This scenario is further supported by the bimodal distribution (two broad peaks at 80° and 100° for $P > 30$ GPa) in the Si–O–Si bridging angle in the same high pressure range. It should be pointed out that the retention of the tetrahedral angle distributions originated from the tetrahedral Si environment is quite evident even up to the highest pressure of 80 GPa which differs from some existing point of view.^{24,48,52,53} A plausible explanation of this is that our near-perfect CRN model with inter-linked tetrahedral units

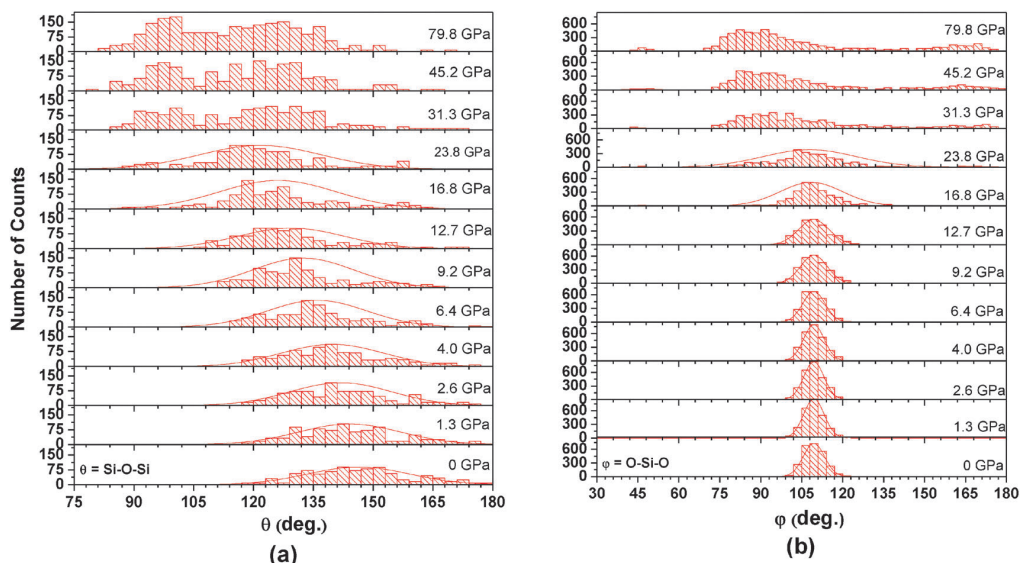


Fig. 4 Distributions of the calculated bond angle vs. pressure: (a) Si–O–Si (θ); (b) O–Si–O (ϕ).

is more resistant to the change in the local structure even at high pressure.

The distribution of Si–O BL as a function of pressure is shown in Fig. 5a and also plotted in Fig. 5b. The initial compression causes a slight shortening of the average the Si–O BL but with an increased spread as expected for the compressed SiO_4 tetrahedra. However, when the pressure goes up to transitional pressures in the range of 20–25 GPa, the average Si–O distance increased abruptly and reaches a maximum of 1.72 Å at 30–35 GPa. This observation of an increase in the Si–O BL

during phase transition is in agreement with the diffraction data of Sato *et al.*^{48,50,51,53,54} which reported a similar increase in the Si–O distance above 10 GPa and reached a maximum at 30 GPa. Our work is also consistent with the work of Benmore,⁵² which also shows the elongation of the Si–O distance commencing at 15 GPa. An interesting point is that at an even higher compression, the overall Si–O distance started to decrease again gradually (see Fig. 5b) due to the compression of the newly formed Si octahedra. This is again in agreement with Sato's work.⁴⁸ We note that unlike these previously reported works,

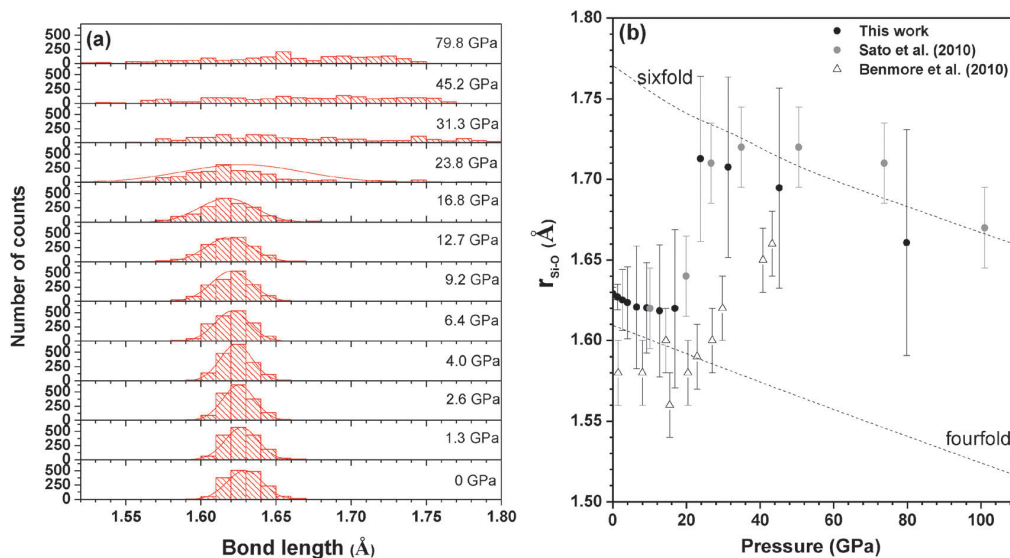


Fig. 5 (a) Distribution of the calculated Si–O bond length vs. pressure, (b) comparison of the average Si–O bond length vs. pressure (black solid circle) with experimental data from Benmore *et al.* (ref. 52 open triangle), and Sato *et al.* (ref. 51, dark solid circle). The error bar for the theoretical curve is the estimated width at the half maximum for distribution in (a).

our simulation shows a wider distribution of the Si–O BL at pressures greater than 35 GPa. Again, this can be attributed to the fact that in our model, there remains a substantial portion of the Si tetrahedral units with non-octahedral environment that can be more effective in enduring compression at higher pressure.

We have also calculated the Si–O coordination number (CN) *versus* pressure based on the integration of the first peak in RPDF (Fig. 3). They are shown in Fig. 6. Our near-perfect CRN glass model retains strictly the 4-fold coordination from zero pressure up to 20–25 GPa, unlike those observed in experiments^{48,51} as well as from MD simulations^{52,55} where the initiation of CN increase took place at a much lower pressure. This again can be attributed to the near-perfect CRN model with no defects thus suppressing the initiation of CN increase with pressure. An increase in CN is noted beyond 20–25 GPa due to the formation of additional Si–O bonds. The increase in CN continues reaching a maximum value of 5.8 at 80 GPa. Similar to the results from the BA and BL distributions discussed above, a change in Si–O CN during the phase transition starts at the same pressure range of 20–25 GPa, and the maximum CN never reached 6 even at the 80 GPa, indicating there remain some structural units with lower CN at the maximum pressure we studied. The presence of additional 5-fold coordination up to 100 GPa has been suggested recently by Sato *et al.*⁵¹ Our finding certainly supports this postulation. On the other hand, recent acoustic velocity data obtained from Brillouin scattering by Murakami and Bass suggested the onset increase in CN from 4 should have started at 30 GPa and that the 6-fold coordination is reached at about 140 GPa.²⁵ These experimental observations suggest that not only the initiation of CN transition, but also the completion of the phase transformation can vary considerably depending on the nature of the initial glass structure and the

subsequent evolution with increasing pressures. Our work demonstrates that with an ideal silica glass network, the phase transition becomes much more gradual with the remnants of lower CN persist even at higher pressure. The extended CN curve (dash line in Fig. 6) hints that there may be a denser phase with higher coordination number (CN) close to 148 GPa.

The structural changes in the simulated glass, although taken place over a much wider pressure range, reflect some of the behavior observed in pressurized crystalline silica⁵ wherein upon compression, the low density crystalline SiO₂ phases (α -quartz and coesite) embedded with tetrahedral clusters are replaced by a sequence of high density silica polymorphs (stishovite \rightarrow orthorhombic CaCl₂ \rightarrow *Pnc2* \rightarrow pyrite). Starting with the stishovite phase which contains distorted octahedral clusters, this phase transition sequence is marked by the increasing and dominant presence of octahedral clusters and networks with a corresponding increase in pressure. At the highest pressure, the pyrite phase also adopts a higher coordination of seven apex polyhedral. Similarly, in the case of crystalline AlPO₄ (berlinite) with structure and bonding isoelectronic with crystalline SiO₂ (α -quartz), such a transformation from tetrahedrally to octahedrally coordinated aluminum phosphate clusters also takes place (at 13 GPa) and at a very high pressure of 97.5 GPa, it transforms into a far more dense phase with a monoclinic structure with a very rare 6-fold bonded PO₆ unit.⁵⁶

B. Mechanical and elastic properties

The elastic and mechanical properties of a-SiO₂ under densification are a subject of great interest.^{57–60} In this paper, we report the results of theoretical calculations of the pressure-dependent elastic properties of a-SiO₂ glass using a strain *vs.* stress analysis method as described in references.^{61,62} This method has been successfully applied to several complex crystals, but not on glasses.^{41–44,63–66} All compressed structures of the a-SiO₂ glass model under pressure are optimized by using VASP. By assuming the near perfect a-SiO₂ model to be close to an orthorhombic cell, the nine components of the stress tensor (C_{11} to C_{66} , C_{12} , C_{13} , and C_{23}) are calculated for each applied strain (ϵ_j). From the set of strain and stress data, the elastic tensor C_{ij} is obtained by solving eqn (1):

$$\sigma_{ij} = \sum_{ij} C_{ij} \epsilon_j \quad (1)$$

From the calculated C_{ij} , the elastic modulus bulk modulus (K), shear modulus (G), Young's modulus (E), and the Poisson's ratio (ν) can be obtained using the Voigt–Reuss–Hill approximation^{67–69} for polycrystals. The calculated elastic coefficients of a-SiO₂ under pressure and K , G , E , ν values are summarized in Table 2 and also plotted in Fig. 7a. Although, amorphous materials are generally considered to be isotropic, in a finite model such as this one, a small degree of anisotropy is expected and will be reflected in the calculated elastic coefficients. Overall, as can be seen in the Fig. 7a, the calculated C_{ij} 's increase with increasing hydrostatic compression as expected but a rapid increase between the 23.8 GPa and 31.3 GPa is particularly interesting. Average rate of change in C_{ij} below

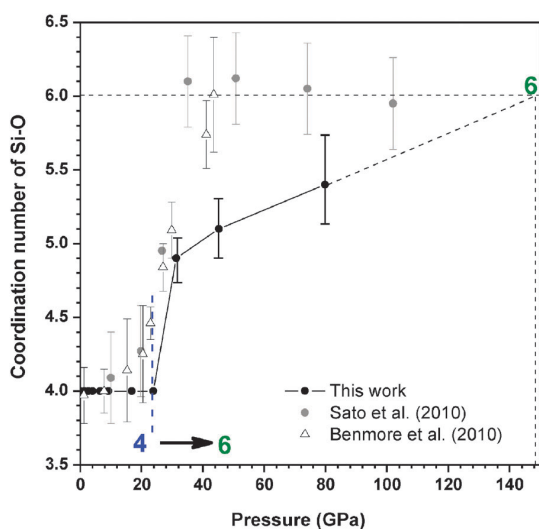


Fig. 6 Comparison of the calculated Si–O coordination number *vs.* pressure (solid circles) with those measured by Benmore *et al.* (ref. 52, open triangle) and Sato *et al.* (ref. 51, dark circles).

Table 2 Elastic modulus (GPa) of the near-perfect CRN model for a-SiO₂ glass upon densification: bulk modulus (K), shear modulus (G), Young's modulus (E), G/K , and Poisson's ratio (ν). The nine elastic constants C_{ij} (GPa)

C_{ij}	Pressure (GPa)											
	P (GPa)											
	0.0	1.3	2.6	4.0	6.4	9.2	12.7	16.8	23.8	31.3	45.2	79.8
C_{11}	102.95	104.82	104.87	104.21	105.68	108.74	124.23	128.61	185.22	385.34	493.22	685.57
C_{22}	92.10	89.72	89.65	92.09	98.20	110.47	131.31	153.89	186.90	341.74	437.57	655.75
C_{33}	102.95	102.38	103.08	104.75	112.40	111.23	122.71	140.40	192.30	239.72	445.65	629.00
C_{44}	36.89	36.58	33.77	35.55	34.22	37.88	39.63	40.93	44.03	68.86	95.42	131.64
C_{55}	40.61	42.00	39.98	40.77	41.94	42.70	45.36	48.54	48.70	90.64	107.32	102.43
C_{66}	37.40	38.22	37.86	36.78	36.69	35.52	37.58	41.58	50.56	97.29	102.72	112.73
C_{12}	18.15	17.97	18.66	20.57	27.06	32.86	46.69	57.79	72.30	187.82	237.35	340.81
C_{13}	24.17	25.70	28.13	30.77	36.66	35.77	49.15	58.82	86.98	173.25	234.91	381.78
C_{23}	15.53	15.87	18.03	20.95	30.19	35.52	49.30	66.57	93.40	165.30	227.84	342.07
Bulk properties												
K (GPa)	45.44	45.58	46.80	49.02	55.65	59.79	74.10	86.57	117.44	217.39	307.00	448.88
G (GPa)	38.64	38.81	37.39	37.61	37.04	38.03	39.73	41.49	48.90	77.46	105.08	119.79
E (GPa)	90.33	90.68	88.59	89.85	90.94	94.13	101.11	107.32	128.80	207.70	282.95	330.00
G/K	0.852	0.851	0.799	0.767	0.667	0.636	0.536	0.479	0.416	0.356	0.342	0.267
ν	0.169	0.168	0.185	0.195	0.228	0.238	0.273	0.293	0.317	0.341	0.346	0.378

23.8 GPa and above 31.3 GPa appears similar and small but a sharp increase of the rate at the pressure range of 23.8 GPa to 31.3 GPa may indicate a major structural change taken place as discussed in the previous sections. Comparison of C_{11} , C_{22} , and C_{33} is a rough estimation for elastic anisotropy. There is a marked increase in elastic anisotropy at 31.3 GPa followed by fairly an isotropic change afterward. This sudden increase in elastic anisotropy at 31.3 GPa could indicate some changes in the orientation of newly formed pentahedra or octahedral groups within the glass model. Another interesting feature in the calculated C_{ij} appears in C_{44} , C_{55} , and C_{66} . Up to 23.8 GPa, they are almost constant and equal to each other. At 31.3 GPa, there is a sudden increase and then somewhat remains constant at higher pressure. Fig. 7b shows the calculated polycrystalline bulk properties of a-SiO₂ with increasing hydrostatic pressure. Since they are calculated from C_{ij} , they show similar variation in trend as in the elastic constants. In addition, one additional observation worth noting is the change in Young's modulus E with pressure. Up to 23.8 GPa, E is larger than bulk modulus B and shear modulus G . But at 31.3 GPa, E is smaller than K even though all three linear elastic constants are increasing. This smaller E results from the fairly constant G beyond 31.3 GPa.

We should note here that the values of elastic properties that we obtained at zero pressure are in general higher than those obtained from previous experimental studies.^{70,71} For example, the estimated value of $(C_{11} + C_{22} + C_{33})/3$ is close to 100 GPa whereas the previous studies showed averaged C_{11} to be close to 75 GPa.⁷¹ As a result, our estimated bulk modulus (~ 44 GPa) is somewhat higher than those of experiment (~ 37 GPa).⁷¹ The overestimation on the C_{11} values may be due to the fact that the presence of the near perfect tetrahedral Si-O environments facilitates an increased resistance toward any bond change in these Si-O tetrahedral clusters. In addition, there has been previous MD simulation studies^{18,19} that demonstrated the presence of an irreversible change in bulk modulus with a subsequent decompression process of a silica glass when it was

subjected to compression up to 20 GPa, yielding a seemingly similar increase in the K value (up to 60 GPa) at ambient temperature and zero pressure. Such an increase in K however is quite distinct from our present high K finding since upon the completion of such compression (up to 20 GPa) and decompression (back to zero pressure), the glass structure from the MD simulations is no longer comprised of the original tetrahedrally coordinated configurations. Rather, the glass structure has irreversibly evolved into a new and denser glass structure wherein the presence of octahedrally coordinated clusters becomes more pronounced and as such, a full recovery to the original glass structure is no longer possible. This is further confirmed by the fact that the density of the decompressed silica glass at zero pressure has in fact arisen to 2.8 g cm⁻³ (from its original 2.2 g cm⁻³ value)¹⁹ and thus, consequently a much higher value of K is obtained.

The phenomenon of an anomalous increase in both bulk modulus and C_{11} in vitreous silica with increasing temperature has been reported in many experimental⁷¹ as well as theoretical studies.^{18,23} It is worthwhile to point out that the maximum values (with temperature) obtained for the zero-pressure K and C_{11} are quite similar to our calculated values; the maximum C_{11} at high temperatures was reported to be close to 95 GPa with a bulk modulus (K) approaching 45 GPa. Previous theoretical study²³ has shown that this anomalous increase and the corresponding maximum values in K and C_{11} are not caused by the thermal-induced stretching of Si-O bond since it would have instead resulted in a decline in both K and C_{11} . Rather, the increase has been attributed to the adjustments associated with both the bond compression and bending behavior of the tetrahedral clusters in the network. Thus, it is possible that our glass model is in fact a representation of an ideal case wherein the rearrangement of the bond compression and bending of vitreous silica has already been optimized by virtue of a nearly perfect tetrahedral environment that is intrinsic to our glass model. A similar case can be obtained apparently by

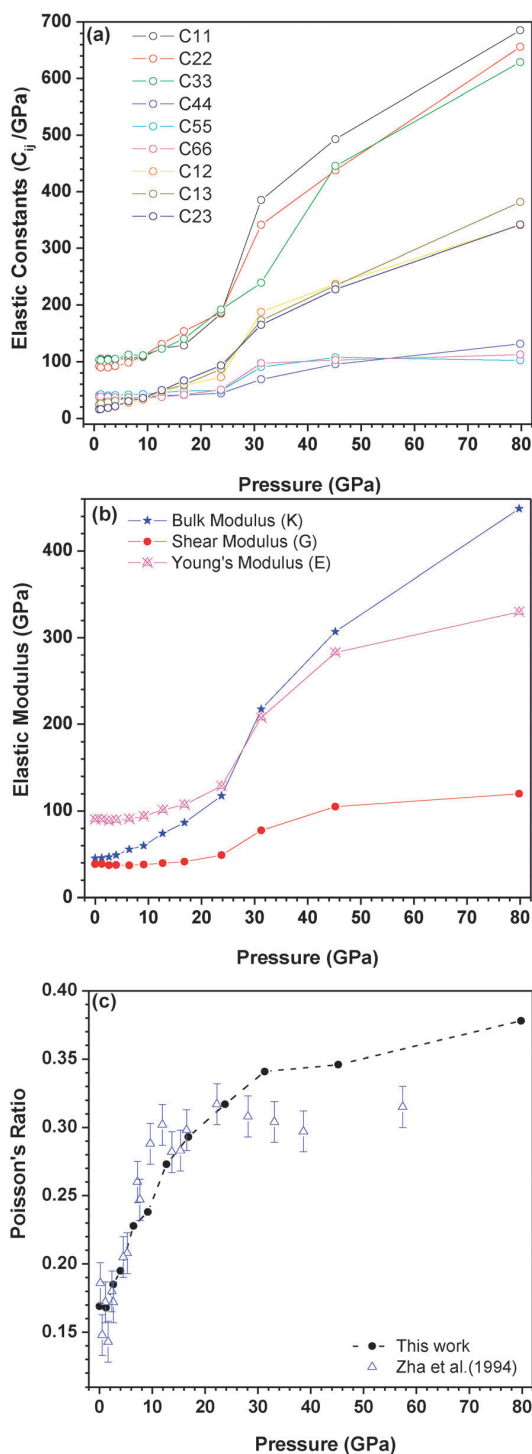


Fig. 7 (a) Calculated elastic constants vs. pressure, (b) calculated elastic moduli vs. pressure, and (c) comparison of the pressure-dependent Poisson's ratio (ν) (solid circles) and the measured data by Zha *et al.* (ref. 47, blue open triangle).

raising the temperature of the silica glass up to a certain temperature before the bond stretching to weaken the mechanical

strength becomes a dominant factor. Indeed, it would be interesting to compare the glass structure possessing the maximum K and C_{11} to our ideal glass structure. This certainly warrants a further detailed comparative study.

The Poisson's ratio (ν) is an important parameter which represents complex mechanical bulk properties of the system. By definition, Poisson's ratio is the negative of the ratio of transverse contraction strain to longitudinal extension strain in the direction of the elastic loading, and as such it is an indication as to how the glass structure can resist change in volume in relation to its resistance to the change in shape. The comparison of the Poisson's ratio vs. pressure obtained from this study and that measured by Zha *et al.*⁴⁷ are shown in Fig. 7c. From this figure, one can see that the Poisson's ratio from Zha's work is shown to increase with increasing pressure up to about 25 GPa, followed by a slight decline beyond 25 GPa. Our results on the other hand show that the Poisson's ratio kept increasing with the corresponding increase in pressure even up to 80 GPa. We do note however that the increase becomes relatively gradual beyond 31 GPa. In previous works,⁵⁹ the increase in Poisson's ratio has been linked to the degree of densification the loss of highly cross-linked atomic network. For silica glass, the sudden raise in Poisson's ratio stems from the transition from tetrahedral to octahedral coordinated clusters, which is completed at 25 GPa in Zha's work.⁴⁷ As the densification becomes more gradual beyond this pressure point, the Poisson's ratio becomes fairly constant accordingly. Unlike Zha's work however, our results show that the Poisson's ratio continues to increase with pressures exceeding 25 GPa. This is due to the fact that the densification process continues to take place even up to the maximum pressure studied (80 GPa) resulting in a concomitant increase in Poisson's ratio. Indeed, the steady increase of the Poisson's ratio beyond 25 GPa in our work appears to be yet another independent indication of the prolonged AAPT as has been similarly observed by the other properties calculated in this study. The complete table of calculated elastic coefficients and mechanical parameters for a-SiO₂ at different pressures are summarized in Table 2.

C. Electron states and interatomic bonding

To elucidate the mechanism of densification of a-SiO₂ glass, we have calculated the electronic structure and bonding in the a-SiO₂ glass models using the OLCAO method. The total density of states (TDOS) as a function of applied pressure is shown in Fig. 8. At zero-pressure, the structure has a band gap of 5.2 eV with local density approximation within the framework of the density functional theory which generally underestimates the true band gap in insulators. This band gap value is in agreement with those reported previously²⁷ and by others.⁷² The band gap does not change appreciably with pressure but reduces slightly as the pressure increases. The occupied portion of the VB consist of the lower segment dominated by the O 2s orbitals with a sharp peak at -17.3 eV and the upper portion from 0 to -10 eV with a well-known mid-gap from -4 to -5 eV separating the upper and lower portion of the VB. Although the real band gap does not change appreciably with pressure, this mid-gap depends

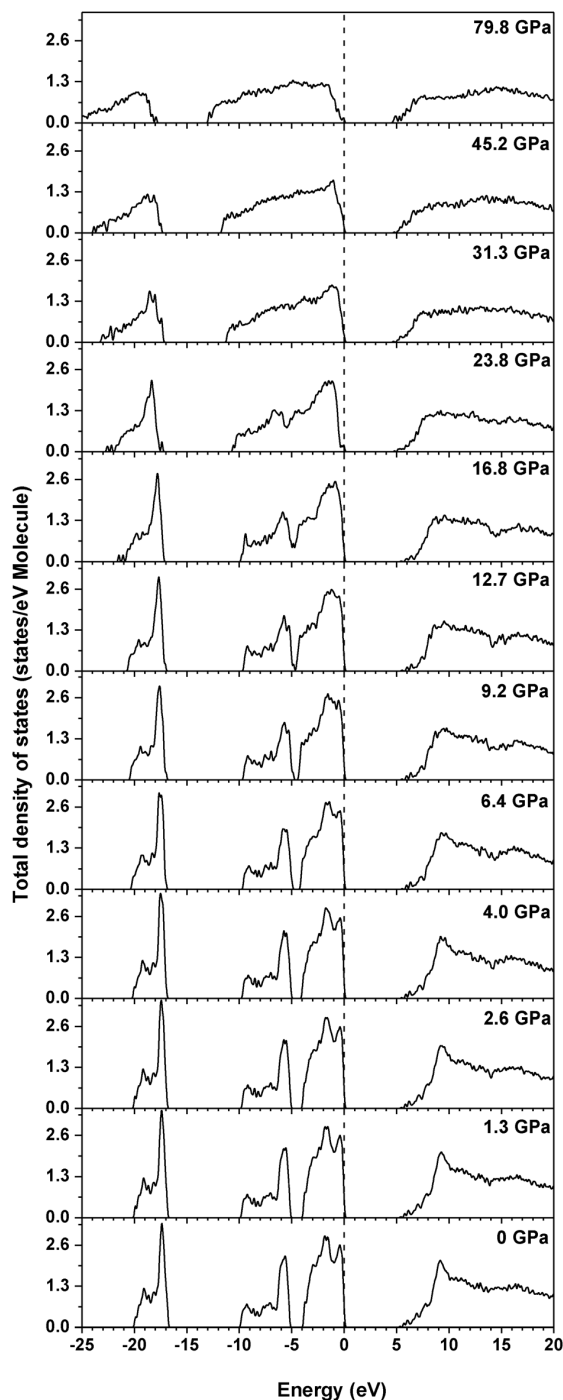


Fig. 8 Calculated total density of states of the a-SiO₂ model vs. pressure. The zero energy is at the top of the valence band (dash line).

sensitively on pressure. It starts to diminish at 12.7 GPa and completely disappears at pressure of 31.3 GPa. There is also a drastic change in the shape of the DOS starting from the pressure in the range of 20 to 35 GPa. Similar drastic change in the shape of the unoccupied CB can also be observed.

To quantitatively investigate the charge transfer, interatomic bonding and localization of electron states at the band edges, we have calculated the effective charge (Q^*), bond order (BO) values and localization index (LI) according to eqn (2)–(4):

$$Q_{\alpha}^* = \sum_i \sum_{n, \text{occ}} \sum_{j, \beta} C_{i\alpha}^{*n} C_{j\beta}^n S_{i\alpha, j\beta} \quad (2)$$

$$\rho_{\alpha\beta} = \sum_{n, \text{occ}} \sum_{i, j} C_{i\alpha}^{*n} C_{j\beta}^n S_{i\alpha, j\beta} \quad (3)$$

$$L_n = \sum_{i, \alpha} \left[\sum_{j, \beta} C_{i\alpha}^{*n} C_{j\beta}^n S_{i\alpha, j\beta} \right]^2 \quad (4)$$

where i and j label the orbital quantum numbers of atoms α and β , and n is the band index. $S_{i\alpha, j\beta}$ is the overlap matrix and $C_{j\beta}^n$ is an eigenvector coefficient of the wave function. In this work, the effective charge of the atom is defined as the number of the valence electrons on this atom based on the Mulliken scheme⁷³ which requires the use of more localized orbital. Hence a minimal basis is used for this purpose. Although it is well known that Mulliken analysis is basis dependent, it is very natural to be used in a method where atomic basis set is used for the expansion and it does not rely on any parameters such as atomic radii of different atoms. This is particularly important in the present study for densification of an amorphous structure since the local environments of each atom are different and they change as pressure increases which make it impossible to accurately quantify the atomic radius of each atom.

Fig. 9a shows the calculated bond order density (defined as the total BO per unit volume) versus pressure in a-SiO₂ glass. The BO density continues to increase with a notable jump at pressure of 20–35 GPa. This increase is similarly linked to the initiation of the amorphous to amorphous phase transition where significant new population of higher coordinated Si start to make contribution to the total bond order. The two-dimensional (“2-D”) and three-dimensional (“3-D”) mapping of the distributions of BO vs. BL (BO–BL) for Si–O bonds up to 2.0 Å for different applied pressures are shown in Fig. 9b and c. As is evident in Fig. 9b, prior to the phase transition, the distribution of BO–BL length is narrowly confined to small region (marked by white circles). This is because for pressure less than 10 GPa, the variations in BL and BO for the nearly perfect tetrahedrally coordinated Si are small. As the pressure increases to about 20–35 GPa, there is a noticeable expansion in the region for BO–BL distribution. This change is consistent with other results confirming the initiation of the AAPT takes place at this pressure range. With further increase in pressure, the BO–BL distribution becomes much more spread-out and exhibiting a well-known inverse relationship in BL vs. BO. Unlike other evidences used to depict phase transition by “1-D” plots, these “2-D” and “3-D” plots can discern more vividly the characteristics of narrow distribution of BL (hence the BO) of the low density amorphous phase. The appearance of the new coordination environment at higher pressure results in not only a wider distribution of the BL, but also a corresponding change in

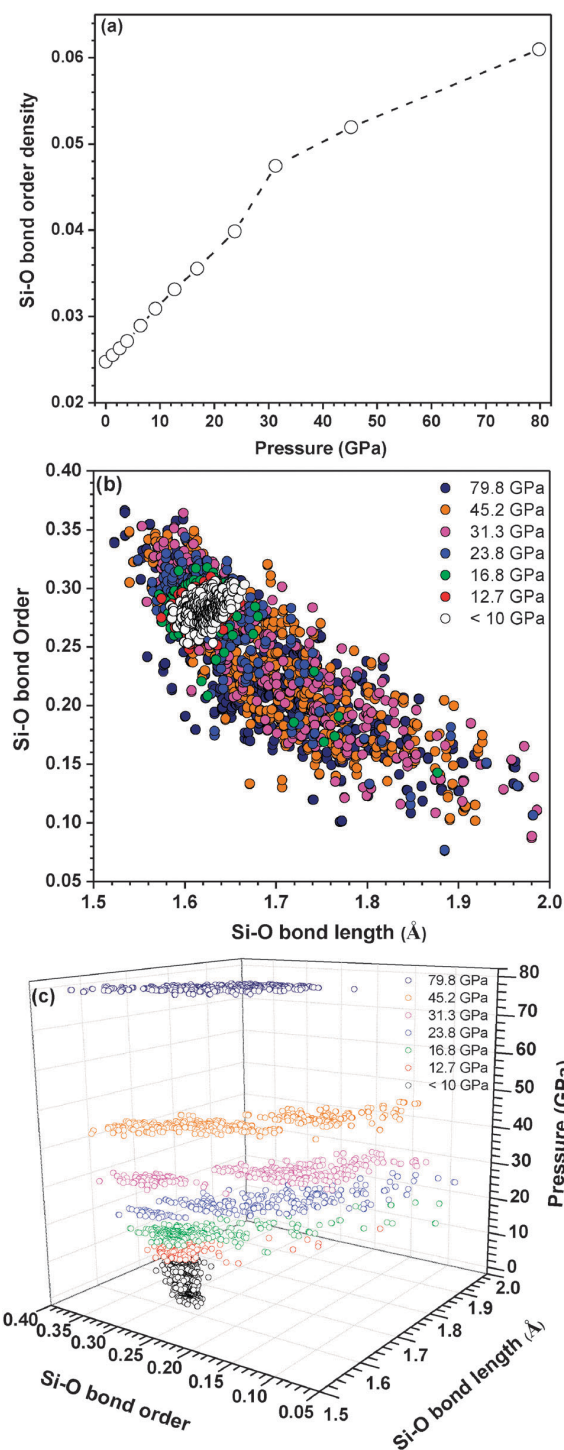


Fig. 9 (a) Calculated Si–O bond order density vs. pressure. (b) A “2-D” mapping of all BO values vs. BL, and (c) a “3-D” mapping plot of (b).

the BO distribution. Hence, our BO–BL distribution plot has the unique capability in providing additional insight on the mechanism of the phase transition in densified a-SiO₂. This is the first

time that we know in which “2-D” and “3-D” BO vs. BL mapping are utilized to elucidate the gradual AAPT mechanism.

The calculated effective charge (Q^*) for Si and O atoms in the model along with its histogram distribution and average values versus pressure are shown in Fig. 10a and b for $P = 0.0, 23.8, 31.3$ and 79.8 GPa. Both Q_{Si}^* and Q_{O}^* have distributions close to a Gaussian form at low pressure ($P < 16.8$ GPa). The distributions became more scattered with an increased pressure. The net charge transfer (defined as the difference between the calculated effective charge Q^* and that of a neutral atom) at different pressure are also summarized in Table 3. Fig. 10 shows that Q_{O}^* increases with pressure while that of Q_{Si}^* reduces. At zero pressure, Si has 1.89 electrons and O has 7.05 electrons on average meaning that there is an average charge transfer of 2.11 electrons from one Si to two O atoms, or 1.05 electrons per O (see Table 3). This is typical of a mixture of ionic and covalent bonds for a system like a-SiO₂ or for other large gap insulators such as Al₂O₃. The average charge transfer from Si to O at pressure of 23.8 GPa, 31.3 GPa and 79.8 GPa are 1.02, 0.99, and 0.97 electrons respectively (see Table 3), indicating a steady decrease in the charge transfer as the pressure increases or the reduction in the ionic component of the bonding with a concomitant increase in the covalent component of the bonding. Thus the densification process of the a-SiO₂ model shows a steady increase in the covalent bonding character as pressure increases. A plot of charge transfer from Si to O as a function of pressure (not shown) indicate that this change is more pronounced in the range of 20–35 GPa, consistent with other signals for the AAPT from a low density phase to a high density phase.

We have also calculated the localization index (LI) for all the electron states in the CRN model of a-SiO₂ glass as a function of pressure. Fig. 11 shows the LI plots for states near the band gap at the pressure of 0.0 GPa, 16.8 GPa, 31.3 GPa and 79.8 GPa, respectively as illustrative examples. As can be seen, the states at near the top of the VB are relatively localized and distributed over a narrow energy range in accordance with the well-established theory of electron localization in non-crystalline solids.⁷⁴ The estimated mobility edge (ME) at $P = 0$. GPa is about 0.10 eV, smaller than the one quoted in the previous calculation using the predecessor of the current model.^{26,27} This is attributed to a much more accurate relaxation of the glass model in the present case with small BL and BA distortions. In a real a-SiO₂ glass, there are always defects and other forms of imperfections that can induce localized states at the band edges which are different from the localized states in a defect-free amorphous structure purely arising from the lack of long range order. On the other hand, numerical estimation of the mobility edge depends on the size of the model. Although the present model with 1296 atoms is the largest that can be done so far, the theoretical limit for the mobility edge at the top of the VB in a-SiO₂ may not have been reached. Fig. 11 also shows that there is no evidence for a mobility edge at the bottom of the CB state is very delocalized as pointed out long time ago.⁷⁵ At higher pressure, mobility edge of the VB increases and the localized states at the

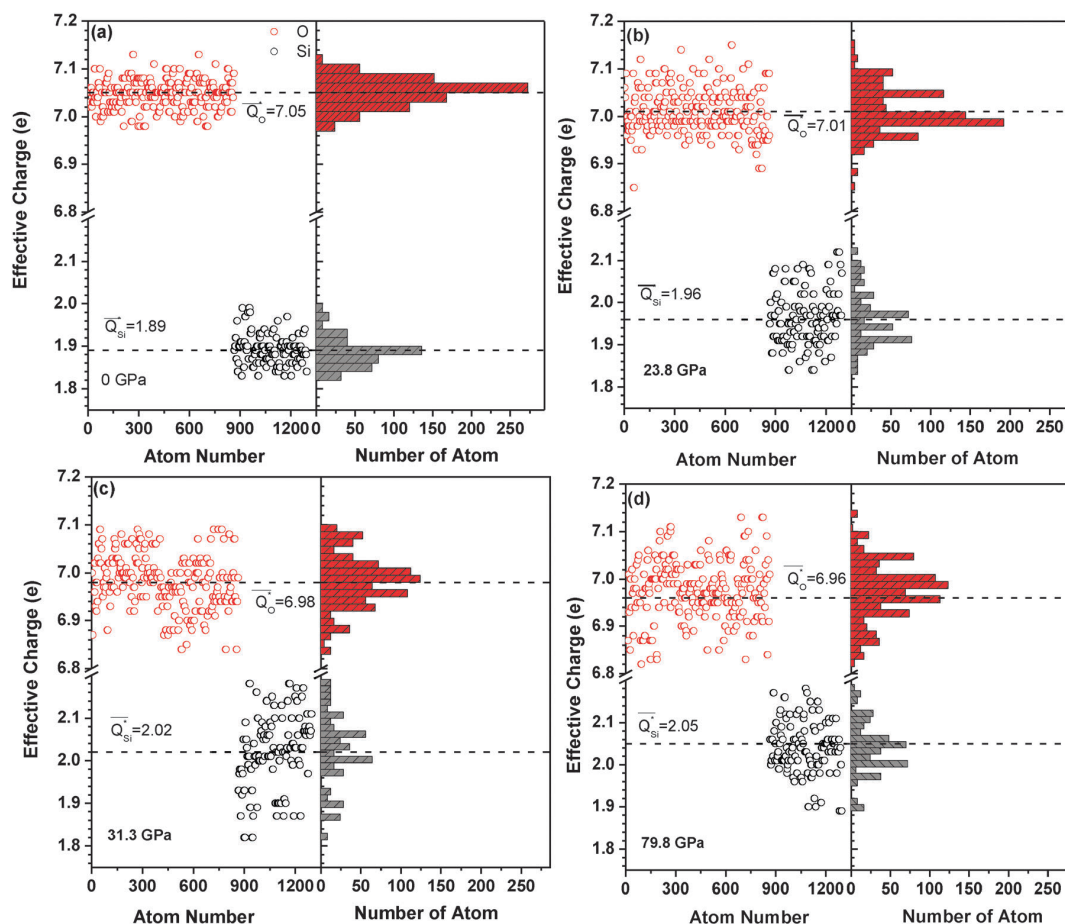


Fig. 10 The calculated effective charge distribution of Si (black circles) and O (red circles) at pressure: (a) 0 GPa, (b) 23.8 GPa, (c) 31.3 GPa, and (d) 79.8 GPa. The dash lines are the averaged values.

Table 3 Calculated net charge transfer (ΔQ^*) (positive means gain electron) and (negative means loss electron) of a-SiO₂ at different pressures

Pressure (GPa)	ΔQ^* (e)	Si	O
0.0		-2.11	1.05
23.8		-2.03	1.02
31.3		-1.97	0.99
79.8		-1.95	0.97

CB edge and start to emerge. This change starts roughly at the pressure of 20–25 GPa where the initiation of amorphous to amorphous transition occurs.

D. Complex dielectric function and refractive index

The interband optical properties of this large CRN a-SiO₂ model under pressure are also calculated in the form of frequency-dependent dielectric function using the OLCAO method. In this calculation, an extended basis set is used which includes one more shell of unoccupied atomic orbitals in the basis set than the full basis set. The use of extended basis set improves the accuracy of the higher CB states and wave functions.

The imaginary part of the dielectric function $\varepsilon_2(\hbar\omega)$ is calculated according to the eqn (5):

$$\varepsilon_2(\hbar\omega) = \frac{e^2}{\pi m \omega^2} \int_{\text{BZ}} d^3k \sum_{n,l} |\langle \psi_n(k,r) | -i\hbar \nabla | \psi_l(k,r) \rangle|^2 \times f_l(k) [1 - f_n(k)] \delta[E_n(k) - E_l(k) - \hbar\omega] \quad (5)$$

where l and n stand for the occupied and unoccupied states, respectively, and $f_l(k)$ and $f_n(k)$ are the Fermi distribution functions. The real part $\varepsilon_1(\hbar\omega)$ is obtained from the imaginary part $\varepsilon_2(\hbar\omega)$ by the Kramers–Kronig transformation.

Fig. 12a shows the calculated dielectric function of a-SiO₂ at $P = 0$ GPa and the experimental spectra using inelastic scattering³² and vacuum ultra-violet spectroscopy.^{33,34} Both experimental data show four clear peaks (marked as P_1 , P_2 , P_3 , and P_4). The strong peak P_1 is the well-known excitonic peak in a-SiO₂. The experimental spectrum at ambient pressure are similar to the earlier measurements by Philipp.^{76,77} The present one-electron calculation of optical properties does not address the excitonic excitation, which is a many-body effect beyond the scope of this paper. Our calculated $\varepsilon_2(\hbar\omega)$ spectrum of zero pressure

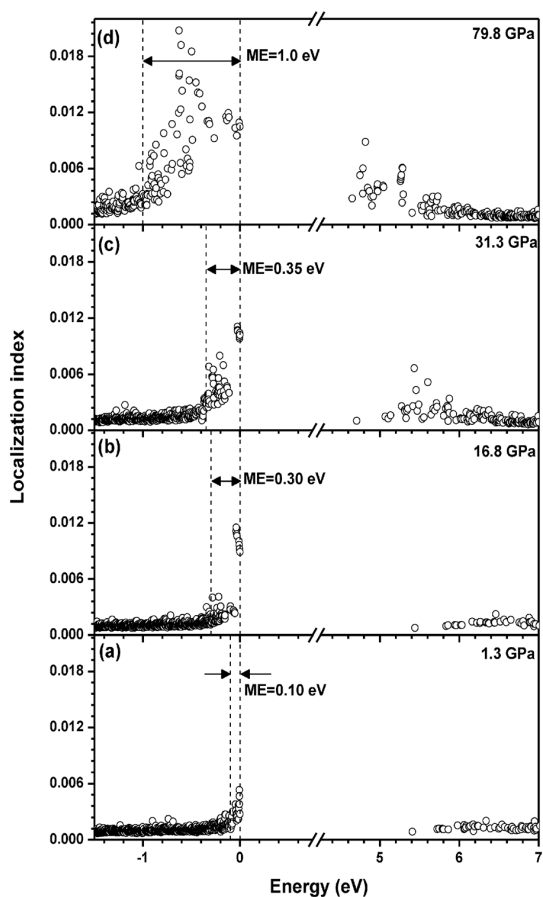


Fig. 11 Calculated localization index of the electron states near the band gap at different pressures: (a) 0 GPa, (b) 16.8 GPa, (c) 31.3 GPa, and (d) 79.8 GPa. "ME" represents "mobility edge" in here.

structure shows three well-resolved peaks at 9.3, 11.6, and 14.6 eV in close agreement with the experimental peaks P_2 , P_3 , P_4 . In this comparison, the experimental curve is shifted downward by 2.56 eV, because the actual absorption edge on-set is masked by the presence of the excitonic peak, and the fact that the one-electron DFT calculation always underestimates the band gap.

The pressure dependent dielectric functions for the a-SiO₂ models are calculated and shown in Fig. 12b. Optical properties changes with increased pressure consistent with changes in the electronic structure. The disappearance of peaks P_1 , P_2 , P_3 under densification at pressure above 20–25 GPa range is noted which coincide with the same pressure range that the AAPT takes place. At the pressure of 79.8 GPa, the absorption curve clearly resembles that of a covalently bonded amorphous semiconductor. We are not aware of any other optical properties calculations on sufficiently large a-SiO₂ glass models, nor the pressure-dependent optical properties.

The refractive index n of the CRN model of a-SiO₂ can be obtained from the square root of the optical dielectric constant $\epsilon_1(0)$, or $n = \sqrt{\epsilon_1(\hbar\omega)}$. At $P = 0$ GPa, we obtained the refractive index of 1.51, in good agreement with different experimentally measured values (see Fig. 13).^{34,47,78–80} The pressure dependence of the refractive index for a-SiO₂ on compression and a least squares fit to the data are shown in Fig. 13. The refractive index of a-SiO₂ glass increases smoothly with pressure in good agreement experimental data.⁴⁷ We have noted that the calculated refractive index under pressure is higher than the experimental data from Zha *et al.*⁴⁷ especially at high pressure range which can be attributed to the fact that our calculation is based on a near-perfect random network model with no defective like structures. Large increase in the refractive index for a-SiO₂ under densification in our calculation is due to change in the fundamental electronic structure, increased covalent bonding

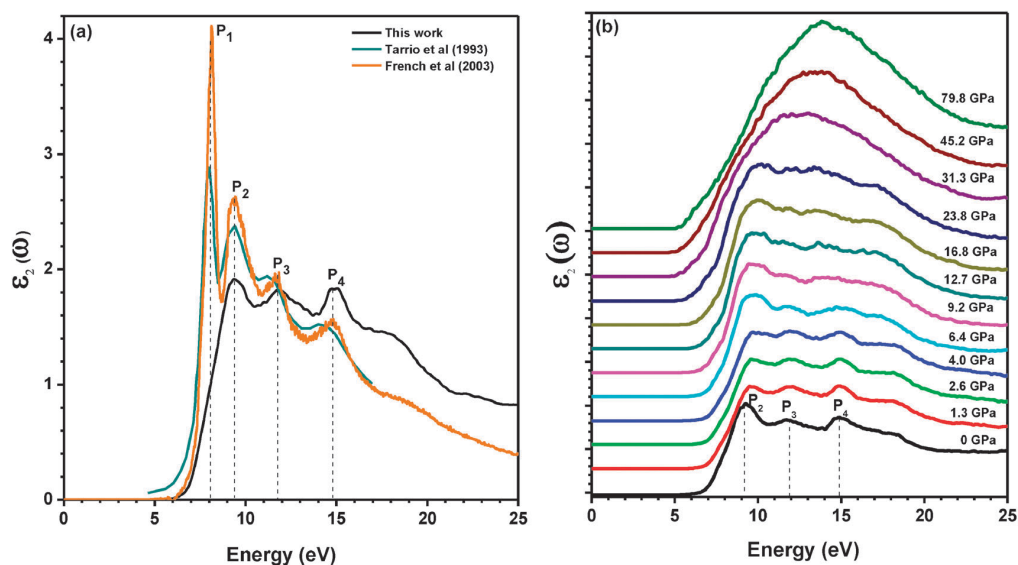


Fig. 12 (a) Comparison of the calculated imaginary part of the dielectric function $\epsilon_2(\hbar\omega)$ at zero pressure (black line) and those measured by Tarrío *et al.* (ref. 32) and French *et al.* (ref. 34). (b) The calculated $\epsilon_2(\hbar\omega)$ as a function of pressure.

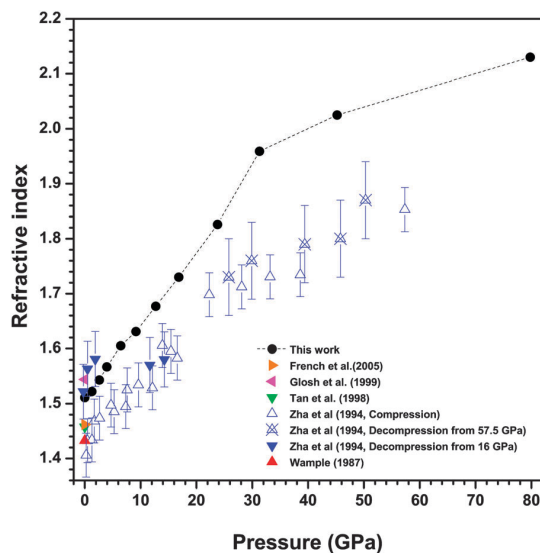


Fig. 13 Comparison of the refractive index vs. pressure from this study (solid circle) and those measured by Zha *et al.* (ref. 47, blue triangle). The refractive index at $P = 0$ GPa measured by French *et al.* (ref. 34, orange triangle), Ghosh *et al.* (ref. 78, pink triangle), Tan *et al.* (ref. 79, green triangle), and Wemple *et al.* (ref. 80, red triangle) are also shown.

character and the slight reduction in the band gap. In addition, Zha⁴⁷ observed two additional findings; (1) the refractive index always increases with pressure during compression mainly due to a continuing increase in density, (2) there is an irreversible change in the density upon decompression of highly compressed silica (up to 57 GPa) caused by a permanent densification taken place between 10–25 GPa which is coinciding with the AAPT. Since we did not perform a decompression simulation in this study, we are unable to replicate the second observation, but our results did show a continuous increase of the index with increasing pressure consistent with his first observation. The magnitudes in our results are however higher than those observed by Zha.⁴⁷ This may be in part due to the fact that the hydroxyl impurities and defects inherent in the silica type II glass used in Zha's experiments to obtain the refractive index as type II glass is typically procured from by fast quenching of melted natural quartz powders. Nevertheless, the trend does show a similar behavior whereby with an accompanying increase in pressure and density, the index consistently increases as well.

V. Conclusions

Based on the fully relaxed near-perfect CRN model of a-SiO₂ glass, the pressure-induced amorphous to amorphous phase transformation (AAPT) of a-SiO₂ has been carefully monitored in this study using a constant-pressure *ab initio* technique. The pressure dependent physical properties including structural, elastic, mechanical, electronic and optical properties are calculated and discussed in the context of atomic scale structural changes and available experimental observations. A distinction between the model used and the real samples in different

experimental measurements and in those obtained from molecular dynamic simulations is emphasized. The importance of having such a near-perfect model with no defective structures should not be dismissed or undervalued since the result obtained based on such a model can serve as the upper limit of many of the measured properties which invariably contains some imperfections in the form of impurities and defects. Our results all point to the presence of amorphous to amorphous phase transformation from a low-density state to a high-density state in a-SiO₂ at a pressure in the range about 20–35 GPa. The changes in the angular distribution functions can be directly related to the increased number of Si atoms with octahedral coordination although we noted the delay in the initiation of the phase transformation due to the fact that the starting silica glass having nearly perfect tetrahedral environments. In addition, the broadening of the bond distance and bond angle distributions can be clearly linked to the increased population of Si and O atoms with higher coordination numbers greater than 4 for Si. We also demonstrated that the changes in the calculated elastic stress tensors can be adapted to probe AAPT. The change in the electronic structure and bonding characteristics together with the interband optical transitions all supports the notion of increased covalent bonding character under compression. This is further confirmed by using the 2-dimensional mapping of bond order vs. bond length distribution that uniquely identifies the initiation of phase transition. Overall, our work substantiated that it is essential to utilize a wide range of changes in glass properties in order to provide a more comprehensive understanding on the nature of the amorphous phase transformation.

It is fitting to comment on further research than can be anticipated using this nearly perfect random network model and the computational approach we used in studying the properties of materials under densification. Firstly, the model can be easily modified to for example, amorphous AlPO₄ glass which has not been studied in detail. In crystalline phase, the electronics structure and phases transitions between alpha quartz and berlinite are remarkably similar. It is not clear if this similarity will be carried over to a-AlPO₄. Many materials in biomolecular systems which are always non-crystalline in nature, contain the PO₄ tetrahedrons as one of the essential structural units and may be mediated by fluids such as water. The model can also be properly modified to study other inorganic glasses such as amorphous B₂O₃ or those glasses with properly added impurities such as Ti or alkali metals for targeted study. The sufficiently large size and the properly maintained directional bounding across the periodic boundaries is a particularly attractive feature for such endeavors. The techniques used for densification and the *ab initio* calculations of the elastic and optical properties under densification can be easily carried over to these similar systems which can certainly reveal many of the interesting and hither to undiscovered features in the physics of non-crystalline solids. Alternatively, one can apply classical MD technique to quench the present near-perfect CRN model from high temperature to investigate the effect of breaking the more ordered network structure with the creation of under- or over-coordinated atoms. It is also desirable to extend the simulation to

decompressing process and in using smaller pressure increments to further improve accuracy. With the rapid advance in computational technology and facilities currently in progress, such large scale *ab initio* simulations no longer face the insurmountable obstacle encountered just a few years ago.

Acknowledgements

This work is supported by U.S. DOE, Office of Basic Energy Sciences, Division of Material Science and Engineering under the award DE-SC008176. This research used the resources of the National Energy Research Scientific Computing Center supported by DOE under Contract No. DE-AC03-76SF00098.

References

- 1 S. R. Elliott, *Physics of amorphous materials*, Longman, London, 1984.
- 2 H. Aoki and Y. Syono, *Physics meets mineralogy: condensed matter physics in the geosciences*, Cambridge University Press, 2000.
- 3 R. Zallen, *The physics of amorphous solids*, Wiley-VCH, 2008.
- 4 P. Richet and P. Gillet, *Eur. J. Mineral.*, 1997, **9**, 907–933.
- 5 L.-G. Liu and W. A. Bassett, *Elements, oxides, and silicates: high-pressure phases with implications for the earth's interior*, Oxford University Press, New York, 1986.
- 6 K. N. Matsukage, Z. Jing and S.-i. Karato, *Nature*, 2005, **438**, 488–491.
- 7 C. Meade, R. J. Hemley and H. K. Mao, *Phys. Rev. Lett.*, 1992, **69**, 1387–1390.
- 8 K. J. Kingma, H.-K. Mao and R. J. Hemley, *High Pressure Res.*, 1996, **14**, 363–374.
- 9 H. Fukui, M. Kanzaki, N. Hiraoka and Y. Q. Cai, *Phys. Rev. B: Condens. Matter Mater. Phys.*, 2008, **78**, 012203.
- 10 S. Susman, K. Volin, D. Price, M. Grimsditch, J. Rino, R. Kalia, P. Vashishta, G. Gwanmesia, Y. Wang and R. Liebermann, *Phys. Rev. B: Condens. Matter*, 1991, **43**, 1194.
- 11 D. Vandembroucq, T. Deschamps, C. Coussa, A. Perriot, E. Barthel, B. Champagnon and C. Martinet, *J. Phys.: Condens. Matter*, 2008, **20**, 485221.
- 12 B. Hehlen, *J. Phys.: Condens. Matter*, 2010, **22**, 025401.
- 13 S. A. Brawer and W. B. White, *J. Chem. Phys.*, 1975, **63**, 2421.
- 14 G. Vaccaro, G. Buscarino, S. Agnello, G. Messina, M. Carpanese and F. Gelardi, *Eur. Phys. J. B*, 2010, **76**, 197–201.
- 15 T. Deschamps, A. Kassir-Bodon, C. Sonnevile, J. Margueritat, C. Martinet, D. de Ligny, A. Mermet and B. Champagnon, *J. Phys.: Condens. Matter*, 2013, **25**, 25402–25405.
- 16 L. Stixrude and M. Bukowinski, *Phys. Rev. B: Condens. Matter*, 1991, **44**, 2523.
- 17 S. T. John, D. D. Klug and Y. Le Page, *Phys. Rev. B: Condens. Matter*, 1992, **46**, 5933.
- 18 L. Huang and J. Kieffer, *Phys. Rev. B: Condens. Matter Mater. Phys.*, 2004, **69**, 224203.
- 19 L. Huang and J. Kieffer, *Phys. Rev. B: Condens. Matter Mater. Phys.*, 2004, **69**, 224204.
- 20 L. Huang, M. Durandurdu and J. Kieffer, *Nat. Mater.*, 2006, **5**, 977–981.
- 21 B. B. Karki, D. Bhattarai and L. Stixrude, *Phys. Rev. B: Condens. Matter Mater. Phys.*, 2007, **76**, 104205.
- 22 Y. Liang, C. R. Miranda and S. Scandolo, *Phys. Rev. B: Condens. Matter Mater. Phys.*, 2007, **75**, 024205.
- 23 B. Liu, J.-Y. Wang, Y.-C. Zhou and F.-Z. Li, *Chin. Phys. Lett.*, 2008, **25**, 2747.
- 24 J.-F. Lin, H. Fukui, D. Prendergast, T. Okuchi, Y. Q. Cai, N. Hiraoka, C.-S. Yoo, A. Trave, P. Eng and M. Y. Hu, *Phys. Rev. B: Condens. Matter Mater. Phys.*, 2007, **75**, 012201.
- 25 M. Murakami and J. D. Bass, *Phys. Rev. Lett.*, 2010, **104**, 025504.
- 26 M.-Z. Huang and W. Ching, *Phys. Rev. B: Condens. Matter*, 1996, **54**, 5299.
- 27 M.-Z. Huang, L. Ouyang and W. Ching, *Phys. Rev. B: Condens. Matter*, 1999, **59**, 3540.
- 28 B. W. H. van Beest, G. J. Kramer and R. A. van Santen, *Phys. Rev. Lett.*, 1990, **64**, 1955–1958.
- 29 S. Tsuneyuki, M. Tsukada, H. Aoki and Y. Matsui, *Phys. Rev. Lett.*, 1988, **61**, 869–872.
- 30 M. J. Sanders, M. Leslie and C. R. A. Catlow, *J. Chem. Soc., Chem. Commun.*, 1984, 1271–1273.
- 31 G. J. Kramer, N. P. Farragher, B. W. H. van Beest and R. A. van Santen, *Phys. Rev. B: Condens. Matter*, 1991, **43**, 5068–5080.
- 32 C. Tarrío and S. Schnatterly, *J. Opt. Soc. Am. B*, 1993, **10**, 952–957.
- 33 G. Tan, M. Lemon and R. French, *J. Am. Ceram. Soc.*, 2003, **86**, 1885–1892.
- 34 G. Tan, M. Lemon, D. Jones and R. French, *Phys. Rev. B: Condens. Matter Mater. Phys.*, 2005, **72**, 205117.
- 35 G. Kresse and J. Furthmüller, *Comput. Mater. Sci.*, 1996, **6**, 15–50.
- 36 G. Kresse and J. Furthmüller, *Phys. Rev. B: Condens. Matter*, 1996, **54**, 11169–11186.
- 37 W. Y. Ching, *J. Am. Ceram. Soc.*, 1990, **73**, 3135–3160.
- 38 W. Y. Ching and P. Rulis, *Electronic Structure Methods for Complex Materials: The Orthogonalized Linear Combination of Atomic Orbitals*, OUP Oxford, 2012.
- 39 P. Hohenberg and W. Kohn, *Phys. Rev.*, 1964, **136**, 864–871.
- 40 W. Kohn and L. J. Sham, *Phys. Rev.*, 1965, **140**, 1133–1138.
- 41 S. Aryal, P. Rulis and W. Ching, *Phys. Rev. B: Condens. Matter Mater. Phys.*, 2011, **84**, 184112.
- 42 S. Aryal, P. Rulis and W.-Y. Ching, *J. Am. Ceram. Soc.*, 2012, **95**, 2075–2088.
- 43 S. Aryal, P. Rulis, L. Ouyang and W. Ching, *Phys. Rev. B: Condens. Matter Mater. Phys.*, 2011, **84**, 174123.
- 44 W. Y. Ching, P. Rulis and A. Misra, *Acta Biomater.*, 2009, **5**, 3067–3075.
- 45 J. P. Perdew, K. Burke and M. Ernzerhof, *Phys. Rev. Lett.*, 1996, **77**, 3865–3868.
- 46 R. S. Mulliken, *J. Chem. Phys.*, 1955, **23**, 1841–1846.
- 47 C.-s. Zha, R. J. Hemley, H.-k. Mao, T. S. Duffy and C. Meade, *Phys. Rev. B: Condens. Matter*, 1994, **50**, 13105–13112.
- 48 T. Sato and N. Funamori, *Phys. Rev. Lett.*, 2008, **101**, 255502.

- 49 M. Wu, Y. Liang, J.-Z. Jiang and S. T. John, *Sci. Rep.*, 2012, **2**, 398.
- 50 D. Wakabayashi, N. Funamori, T. Sato and T. Taniguchi, *Phys. Rev. B: Condens. Matter Mater. Phys.*, 2011, **84**, 144103.
- 51 T. Sato and N. Funamori, *Phys. Rev. B: Condens. Matter Mater. Phys.*, 2010, **82**, 184102.
- 52 C. Benmore, E. Soignard, S. Amin, M. Guthrie, S. Shastri, P. Lee and J. Yarger, *Phys. Rev. B: Condens. Matter Mater. Phys.*, 2010, **81**, 054105.
- 53 N. Funamori and T. Sato, *Earth Planet. Sci. Lett.*, 2010, **295**, 435–440.
- 54 N. Funamori and T. Sato, *Phys. Rev. Lett.*, 2009, **102**, 209604.
- 55 R. G. Della Valle and E. Venuti, *Phys. Rev. B: Condens. Matter*, 1996, **54**, 3809–3816.
- 56 J. Pellicer-Porres, A. M. Saitta, A. Polian, J. P. Itie and M. Hanfland, *Nat. Mater.*, 2007, **6**, 698–702.
- 57 V. Keryvin, J.-X. Meng, S. Gicquel, J.-P. Guin, L. Charleux, J.-C. Sangleboeuf, P. Pilvin, T. Rouxel and G. L. Quilliec, arXiv preprint arXiv:1303.6693, 2013.
- 58 T. Rouxel, H. Ji, J. Guin, F. Augereau and B. Ruffle, *J. Appl. Phys.*, 2010, **107**, 094903.
- 59 T. Rouxel, H. Ji, T. Hammouda and A. Moréac, *Phys. Rev. Lett.*, 2008, **100**, 225501.
- 60 T. Rouxel, H. Ji, V. Keryvin, T. Hammouda and S. Yoshida, *Adv. Mater. Res.*, 2008, **39**, 137–146.
- 61 O. H. Nielsen and R. M. Martin, *Phys. Rev. Lett.*, 1983, **50**, 697–700.
- 62 H. Yao, L. Ouyang and W.-Y. Ching, *J. Am. Ceram. Soc.*, 2007, **90**, 3194–3204.
- 63 W. Y. Ching, L. Ouyang, P. Rulis and H. Yao, *Phys. Rev. B: Condens. Matter Mater. Phys.*, 2008, **78**, 014106.
- 64 W. Y. Ching, P. Rulis, L. Ouyang, S. Aryal and A. Misra, *Phys. Rev. B: Condens. Matter Mater. Phys.*, 2010, **81**, 214120.
- 65 L. Liang, P. Rulis and W. Y. Ching, *Acta Biomater.*, 2010, **6**, 3763–3771.
- 66 W. Y. Ching, S. Aryal, P. Rulis and W. Schnick, *Phys. Rev. B: Condens. Matter Mater. Phys.*, 2011, **83**, 155109.
- 67 W. Voigt, *Lehrbuch der Kristallphysik*, Teubner, Leipzig, 1928.
- 68 A. Reuss, *J. Appl. Math. Mech./Z. Angew. Math. Mech.*, 1929, **9**, 49–58.
- 69 R. Hill, *Proc. Phys. Soc., London, Sect. A*, 1952, **65**, 349.
- 70 R. L. Parc, V. Ranieri, J. Haines, M. Cambon, O. Cambon, C. Levelut and S. Clément, *J. Phys.: Condens. Matter*, 2009, **21**, 375109.
- 71 A. Polian, V.-T. Dung and P. Richet, *Europhys. Lett.*, 2002, **57**, 375.
- 72 T. Tamura, S. Ishibashi, S. Tanaka, M. Kohyama and M.-H. Lee, *Phys. Rev. B: Condens. Matter Mater. Phys.*, 2008, **77**, 085207.
- 73 R. Mulliken, *J. Chem. Phys.*, 1955, **23**, 2343.
- 74 P. W. Anderson, *Phys. Rev.*, 1958, **109**, 1492–1505.
- 75 W. Y. Ching, *Phys. Rev. Lett.*, 1981, **46**, 607–610.
- 76 H. Philipp, *J. Phys. Chem. Solids*, 1971, **32**, 1935–1945.
- 77 H. R. Philipp, *J. Non-Cryst. Solids*, 1972, **8–10**, 627–632.
- 78 G. Ghosh, *Opt. Commun.*, 1999, **163**, 95–102.
- 79 C. Z. Tan, J. Arndt and H. S. Xie, *Phys. B*, 1998, **252**, 28–33.
- 80 S. H. Wemple, *Phys. Rev. B: Solid State*, 1973, **7**, 3767–3777.